AIP | Journal of Applied Physics

Self-consistent gain analysis of type-II 'W' InGaN–GaNAs quantum well lasers

Hongping Zhao, Ronald A. Arif, and Nelson Tansu

Citation: J. Appl. Phys. **104**, 043104 (2008); doi: 10.1063/1.2970107
View online: http://dx.doi.org/10.1063/1.2970107
View Table of Contents: http://jap.aip.org/resource/1/JAPIAU/v104/i4
Published by the American Institute of Physics.

Self-consistent gain analysis of type-II '*W*' InGaN–GaNAs quantum well lasers

Hongping Zhao,[a] Ronald A. Arif, and Nelson Tansu[b]
Center for Optical Technologies, Department of Electrical and Computer Engineering, Lehigh University, 7 Asa Drive, Bethlehem, Pennsylvania 18015, USA

(Received 26 May 2008; accepted 18 June 2008; published online 27 August 2008)

Type-II InGaN–GaNAs quantum wells (QWs) with thin dilute-As (~3%) GaNAs layer are analyzed self-consistently as improved III-nitride gain media for diode lasers. The band structure is calculated by using a six-band $\boldsymbol{k}\cdot\boldsymbol{p}$ formalism, taking into account valence band mixing, strain effect, spontaneous and piezoelectric polarizations, as well as the carrier screening effect. The type-II InGaN–GaNAs QW structure allows large electron-hole wave function overlap by confining the hole wave function in the GaNAs layer of the QW. The findings based on self-consistent analysis indicate that type-II InGaN-GaNAs QW active region results in superior performance for laser diodes, in comparison to that of conventional InGaN QW. Both the spontaneous emission radiative recombination rate and optical gain of type-II InGaN–GaNAs QW structure are significantly enhanced. Reduction in the threshold current density of InGaN–GaNAs QW lasers is also predicted. © *2008 American Institute of Physics*. [DOI: 10.1063/1.2970107]

I. INTRODUCTION

Low-threshold diode lasers and high-efficiency light emitting diodes (LEDs) based on III-nitride semiconductor are of great interest for applications in medical diagnostics, optical storage, full color display, and solid state lighting.[1–3] In III-nitride semiconductor material systems, there are several major challenges that prevent high performance conventional InGaN quantum well (QW) LEDs and lasers, as follows: (1) high strain misfit result from the lattice mismatch between the InGaN QW and GaN barriers, (2) large phase separation in high In-content InGaN QW, and (3) charge separation due to the existence of the built-in electric field inside the QW. The built-in electric field in the InGaN-based QW is a result of the existence of both spontaneous and piezoelectric polarization fields in the *c*-plane nitride material systems. The electrostatic field in the QW leads to the spatial charge separation of the electron and hole wave functions, which reduces the transition matrix element of the QW. The reduced electron-hole wave function overlap (Γ_{e_hh}) as a result of the polarization fields inside the InGaN QW leads to a significant reduction in the radiative recombination rate and optical gain of the conventional InGaN QW. The limitations in the InGaN QW active regions lead to a high threshold current density in the state-of-the-art nitride-based diode lasers. As the In content in the QW is increased to extend the emission wavelength, the threshold current density will increase significantly in particular for diode lasers emitting in the blue-green regime ($J_{th}\sim 1.5$ kA/cm^2 for $\lambda\sim 425$ nm and $J_{th}\sim 6$ kA/cm^2 for $\lambda\sim 482$ nm).[4]

Recently, several approaches have been attempted to reduce the charge separation effect by implementing the following: (1) the growth of nonpolar $(11\bar{2}0)$ InGaN QW,[5] (2) δ-AlGaN layer in the InGaN QW,[6,7] (3) staggered InGaN QW structure,[8–10] (4) strain-compensated InGaN–AlGaN QW,[11–13] and (5) type-II InGaN–GaNAs QW.[14] The approaches based on these QW designs with improved electron-hole wave function overlap (Γ_{e_hh}) enable the enhancement in the radiative efficiency of the InGaN-based QW and output power of LED devices.[5–10,13]

The concept of type-II '*W*' QW active region was first proposed and demonstrated by Meyer and co-workers[15,16] in the GaSb material system for midinfrared lasers. Currently state-of-the-art GaSb-based type-II QW lasers have been demonstrated as among the leading diode lasers in the midinfrared regimes. Recently, dilute-nitride type-II '*W*' QW active regions have also been proposed and demonstrated for laser applications in the 1550 nm (Refs. 17–19) and 3–5 μm (Ref. 20) regimes on GaAs and InP substrates, respectively. Recently, we proposed the use of type-II InGaN–GaNAs QW active region to reduce charge separation effect in the visible nitride-based QW,[14] by confining the hole wave function in the dilute-As GaNAs QW layer. However, the analysis presented in Ref. 14 did not take into account the carrier screening effect, which could lead to an underestimation of the optical gain for the nitride QW active regions.

In this paper, we present the self-consistent analysis of type-II InGaN–GaNAs QW active region for diode lasers applications. The energy dispersion relation of the band structure is calculated based on a six-band $\boldsymbol{k}\cdot\boldsymbol{p}$ formalism for wurtzite semiconductor,[21] which takes into account the strain effect, valence band mixing, polarization fields, and the carrier screening effect. In this work, we analyzed and compared both the spontaneous emission and optical gain characteristics of type-II InGaN–GaNAs QW and conventional type-I InGaN QW active regions for lasers applications, taking into account the carrier screening effect by using the self-consistent model. In our studies, both active regions were designed for diode lasers to emit at an emission wavelength of $\lambda_{lasing}\sim 460$ nm. Threshold analyses for both ac-

[a]Electronic mail: hoz207@lehigh.edu.
[b]Electronic mail: tansu@lehigh.edu.

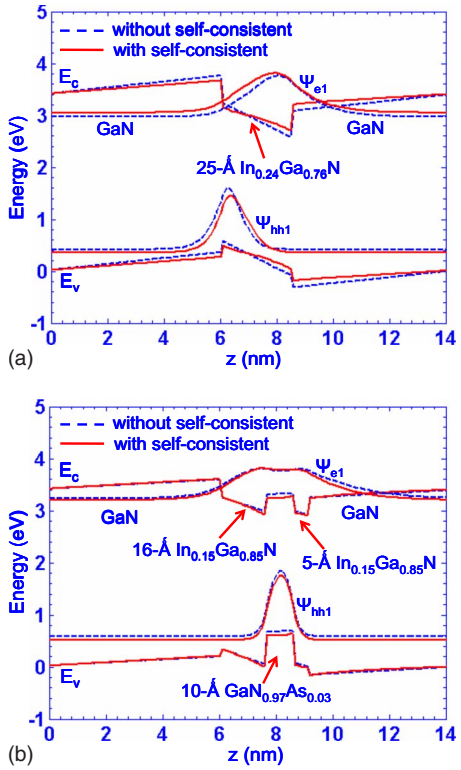

FIG. 1. (Color online) Energy band lineups and wave functions of (a) type-I $In_{0.24}Ga_{0.76}N$ QW and (b) type-II $In_{0.15}Ga_{0.85}N$-$GaN_{0.97}As_{0.03}$ QW. Solid lines correspond to self-consistent calculation by taking into account the carrier screening effect (for $n=5\times10^{19}$ cm^{-3}). Dash lines correspond to band lineups without self-consistent calculation.

tive regions were also compared to investigate the feasibility of the implementation of type-II InGaN–GaNAs QW as the active region for visible nitride laser diodes.

II. CONCEPT OF TYPE-II INGAN–GANAS QWS

Figures 1(a) and 1(b) show the energy band diagrams for both type-I InGaN QW and type-II InGaN–GaNAs QW structures with (solid line) and without (dash line) self-consistent calculation. The self-consistent energy band diagram in Figs. 1(a) and 1(b) were calculated for carrier density (n) at $n=5\times10^{19}$ cm^{-3}. The conventional QW active region structure utilizes 25 Å $In_{0.24}Ga_{0.76}N$ QW with GaN barriers, as shown in Fig. 1(a). The type-II 'W' QW active region employs a 10 Å $GaN_{0.97}As_{0.03}$ layer sandwiched by 16 Å $In_{0.15}Ga_{0.85}N$ and 5 Å $In_{0.15}Ga_{0.85}N$ QW layers, as shown in Fig. 1(b). By utilizing the type-II QW structure, the hole wave function is pushed to the GaNAs layer of the QW active layer, which leads to higher electron-hole wave functions overlap as compared to the type-I InGaN QW. Both the type-I and type-II structures are designed to emit at the same wavelength for laser applications [$\lambda_{peak}\sim460$ nm at near-threshold condition, $n_{th}\sim(2.4-3.8)\times10^{19}$ cm^{-3}]. Our studies indicate that the carrier screening effect should be taken into account when the carrier density (n) is above $\sim1\times10^{19}$ cm^{-3},[13] which is important for laser applications. As shown in Figs. 1(a) and 1(b), the consideration of carrier screening effect leads to the flattening of the band lineups. Due to the improved hole confinement in the dilute-As GaNAs layer in the type-II QW structure, its electron-hole wave function overlap is expected to increase. In the type-II QW structure shown in Fig. 1(b), the electron-hole wave function overlap (Γ_{e_hh}) is calculated as 57.63%, which is improved by 2.09 times of that of conventional InGaN QW [$\Gamma_{e\_hh}=27.48\%$, Fig. 1(a)]. The improved electron-hole wave function overlap (Γ_{e_hh}) in type-II QW active region will lead to a significantly improved transition matrix element, which is proportional to $|\Gamma_{e\_hh}|^2$.

It is important to note that the proposed type-II QW structure employ thin (1 nm) GaNAs layer with low As content (As$<5\%$). The growth in single-phase wurtzite GaNAs alloy had been recently demonstrated by metal-organic chemical vapor deposition by Kimura *et al.*[22] Recent studies by Wu *et al.*[23] show that the incorporation of dilute As into the GaN alloy shows hybridization of the localized As states and the GaN valence band. The valence band hybridization in GaNAs leads to a formation of a new valence band with transitional gap of the N-rich GaNAs lying between 2.5 and 2.7 eV,[23] which also in turn leads to an increase in the valence band offset in dilute-As GaNAs/GaN heterojunction.[23]

III. THEORETICAL AND NUMERICAL FORMULATION OF SELF-CONSISTENT MODEL

The calculation of the band structure is based on a six-band $\boldsymbol{k}\cdot\boldsymbol{p}$ formalism for wurtzite semiconductors,[21,24] without considering the coupling between the conduction band and valence band. This assumption is reasonable as the coupling between the conduction and valence bands are minimal for the case of wide band gap semiconductor systems.[21,24] The numerical model takes into account the valence band mixing, the strain effect, and the spontaneous and piezoelectric polarizations,[25] as well as the carrier screening effect.[13] Schrodinger's and Poisson's equations are calculated iteratively until the eigenenergy converges. The calculation of the spontaneous emission rate takes into account both the TE and TM polarizations. The optical gain is calculated for TE polarization due to the negligibility of the optical gain for TM polarization. The details of the self-consistent numerical model for InGaN-based QW active regions employing six-band $\boldsymbol{k}\cdot\boldsymbol{p}$ formalism are presented in Ref. 13.

The material parameters of the wurtzite III-nitride semiconductor used in the band structure calculations are obtained from Refs. 26–31. These parameters are shown in Table I. The material parameters of the ternary alloys use the linear interpolation of that of the binary InN and GaN, except for the energy band gap of InGaN alloys. In our analysis, the energy band gap of $In_xGa_{1-x}N$ alloy is computed by employing bowing parameter of 1.4 eV (Refs. 27 and 29) and InN energy gap of 0.6405 eV.[27,29]

In developing the valence band hybridization model of N-rich GaNAs alloy, a flat conduction band alignment was assumed between GaN and GaNAs similar to the finding in Ref. 23. The energy band gap of the dilute-As $GaN_{1-y}As_y$ alloy can be obtained from linear extrapolation of the experimental data shown in Ref. 23 for low As content (y) up to 6.7%, as follows (in eV):

TABLE I. Material parameters for GaN and InN. The values are taken from Refs. 26–31.

Parameters	GaN	InN
Lattice constant (Å)		
a	3.189	3.548
Energy parameters		
E_g(eV) at 300 K	3.42	0.6405
$\Delta_1(=\Delta_{cr})$(eV)	0.019	0.041
$\Delta_1=\Delta_2=\Delta_{so}/3$(eV)	0.014	0.001
Conduction-band effective masses		
$m^*_{//}/m_0$ at 300 K	0.18	0.11
$m^*_{\perp}/m_0$ at 300 K	0.20	0.11
Valence-band effective mass parameters		
A_1	−7.24	−9.24
A_2	−0.51	−0.6
A_3	6.73	8.68
A_4	−3.36	−4.34
A_5	−3.40	−1.47
A_6	−4.90	−1.64
Deformation potentials		
a_c(eV)	−4.08	−4.08
D_1(eV)	0.7	0.7
D_2(eV)	2.1	2.1
D_3(eV)	1.4	1.4
D_4(eV)	−0.7	−0.7
Elastic stiffness constants		
C_{11}(GPa)	390	223
C_{12}(GPa)	145	115
C_{13}(GPa)	100	124
C_{33}(GPa)	392	182
Piezoelectric coefficients		
d_{13}(pm V^{-1})	−1.0	−3.5
d_{33}(pm V^{-1})	1.9	7.6
Spontaneous polarization		
$P_{sp}(C/m^2)$	−0.034	−0.042

$$E_{g\_GaNAs}(y) = -4.565y + 2.7978 \quad (\text{for } 0 < y < 0.067). \tag{1}$$

The finite difference method is used to solve the Schrödinger equations for semiconductor heterostructure/nanostructure.[13,21] The step size for the finite difference method is 1 Å. The carrier distribution in the QW will influence the band-edge potential, and vice versa. Therefore, to take into account the carrier screening effect, both the band-edge potential and carrier distribution in the QW have to be solved self-consistently based on the Poisson equation. The convergence condition in this calculation is set such as the tolerance of the eigenenergy is less than 0.1%, which requires 10–15 iterations for each carrier density.

IV. MOMENTUM MATRIX ELEMENTS CHARACTERISTICS OF TYPE-II INGAN–GANAS QW

Figures 2(a) and 2(b) show the square of momentum matrix elements for TE-polarization transitions as a function of in-plane wave vector (k_t) for both type-I InGaN QW and type-II InGaN–GaNAs QW, respectively. The square of the transition matrix elements for C1-HH1, C1-LH1, C1-HH2, C1-LH2, C2-HH1, C2-LH1, C2-HH2, and C2-LH2 transitions are compared at a carrier density of $n=3\times10^{19}$ cm^{-3}. From Figs. 2(a) and 2(b), the C-HH and C-LH momentum matrix elements are similar at the zone center ($k_t=0$). However, as the increase in the wave vector, the momentum matrix elements of C-HH and C-LH transitions diverge. Note that the momentum matrix elements for C1-HH1 and C1-LH1, which are the transitions that dominantly contribute to spontaneous emission rate (R_{sp}), are improved for type-II QW as compared to those of type-I QW.

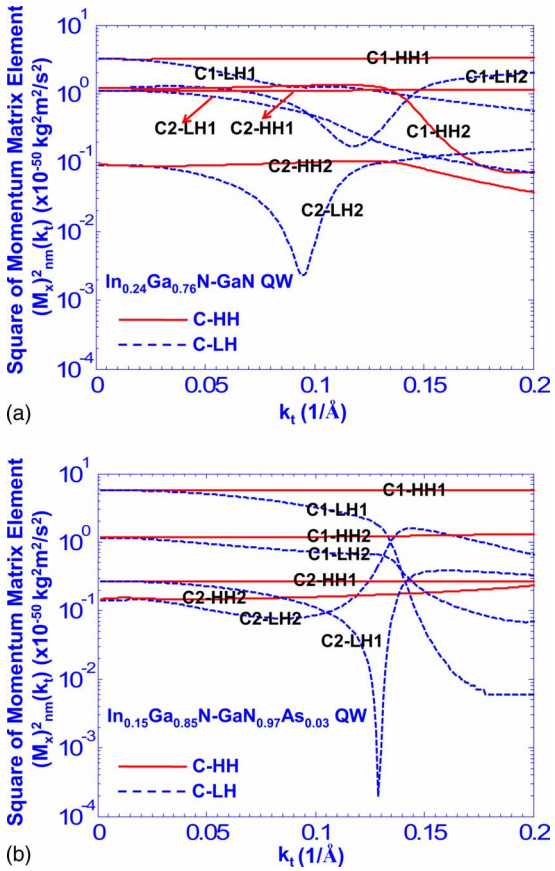

FIG. 2. (Color online) Square of momentum matrix elements as a function of the in-plane wave vector k_t in the TE polarization for (a) type-I $In_{0.24}Ga_{0.76}N-GaN$ QW and (b) type-II $In_{0.15}Ga_{0.85}N-GaN_{0.97}As_{0.03}$ QW. The carrier density is 3×10^{19} cm^{-3}.

The square of momentum matrix elements at the zone center ($k_t=0$) as a function of the carrier density for type-I and type-II QWs are shown in Figs. 3(a) and 3(b). Note that the momentum matrix elements for C-HH and C-LH with the same quantum number are similar for each carrier density at the zone center ($k_t=0$). For both type-I and type-II QWs, the matrix elements for C1-HH1, C1-LH1, C1-HH2, and C1-LH2 increase as the carrier density increases. However, the matrix elements for C2-HH1, C2-LH1, C2-HH2, and C2-LH2 are relatively unchanged, as the carrier density increases. The matrix elements for C1-HH1 and C1-LH1 transitions in type-II QW are much higher than those of the type-I QW, which are the main factors leading to the significant improvement in the spontaneous emission rate and optical gain for type-II QW.

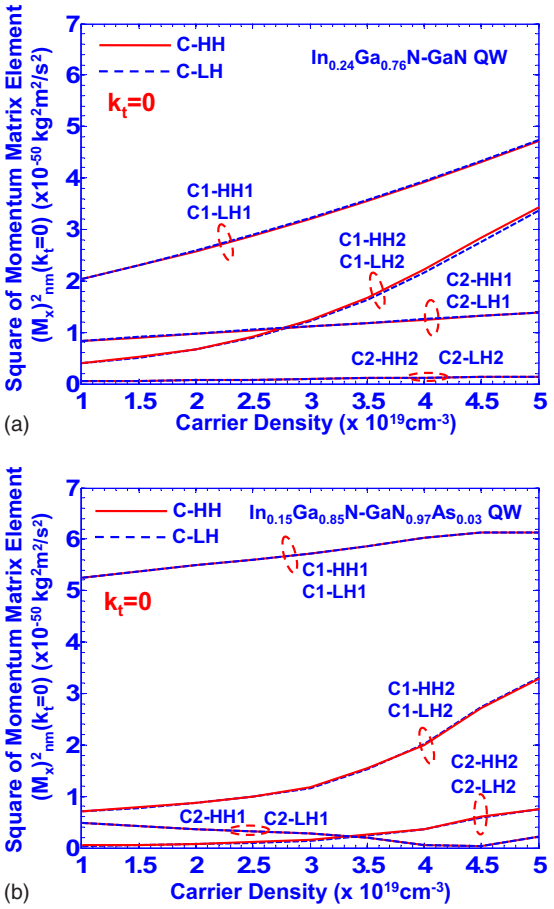

FIG. 3. (Color online) Square of momentum matrix elements at zone center ($k_t=0$) using the self-consistent model as a function of the carrier density for (a) type-I $In_{0.24}Ga_{0.76}N-GaN$ QW and (b) type-II $In_{0.15}Ga_{0.85}N-GaN_{0.97}As_{0.03}$ QW.

V. SPONTANEOUS EMISSION CHARACTERISTICS OF TYPE-II INGAN–GANAS QW

The room-temperature spontaneous emission spectra of the type-I $In_{0.24}Ga_{0.76}N-GaN$ QW and type-II $In_{0.15}Ga_{0.85}N-GaN_{0.97}As_{0.03}$ QW structures were calculated and compared for carrier density (n) from 1×10^{19} up to 5×10^{19} cm^{-3} at $T=300$ K, as shown in Fig. 4. Note that the spontaneous emission spectra were calculated taking into consideration the carrier screening effect from the self-consistent model. The consideration of carrier screening effect is important for the carrier density above 1×10^{19} cm^{-3}.[9,13] As shown in Fig. 4, both the type-I and type-II QW structures show a blueshift of the peak of spontaneous emission spectra as the carrier density increases, primarily due to the carrier screening effect (for $n>1\times10^{19}$ cm^{-3}). As the carrier density in the QW is increased, stronger blueshift in the peak emission wavelength is observed for the type-I InGaN QW structure resulting in shift from $\lambda=480$ nm ($n=1\times10^{19}$ cm^{-3}) to $\lambda=457$ nm ($n=5\times10^{19}$ cm^{-3}). Less carrier screening effect is observed in the type-II QW, which result in a minimal blueshift as the carrier density is increased in the QW. For the type-II InGaN–GaNAs QW, we found that the emission wavelength shifts from $\lambda=464$ nm ($n=1\times10^{19}$ cm^{-3}) to 456 nm ($n=5\times10^{19}$ cm^{-3}).

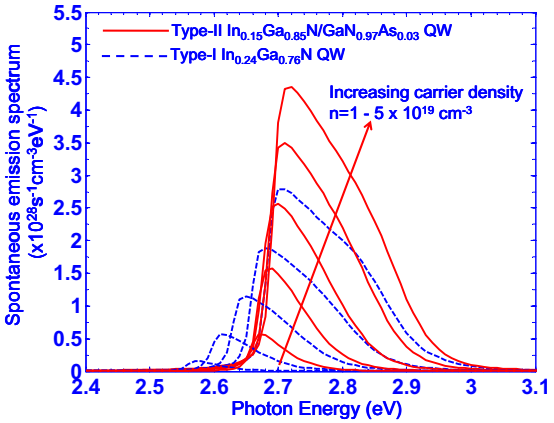

FIG. 4. (Color online) Spontaneous emission spectra for type-I $In_{0.24}Ga_{0.76}N$ QW and type-II $In_{0.15}Ga_{0.85}N-GaN_{0.97}As_{0.03}$ QW as increasing carrier density $n=(1-5)\times10^{19}$ cm^{-3} with self-consistent model calculation.

The spontaneous emission spectra of the type-II InGaN–GaNAs QW show significant improvement as compared to the type-I InGaN QW. At $n=2\times10^{19}$ cm^{-3} ($n=5\times10^{19}$ cm^{-3}), the peak spontaneous emission spectra of the type-II InGaN–GaNAs QW structure is 1.57×10^{28} s^{-1} cm^{-3} eV^{-1} (4.35×10^{28} s^{-1} cm^{-3} eV^{-1}), which is approximately 2.8 times (1.56 times) higher than that of the type-I InGaN QW of 5.62×10^{27} s^{-1} cm^{-3} eV^{-1} (2.79×10^{28} s^{-1} cm^{-3} eV^{-1}). The improvement in the spontaneous emission radiative recombination rate for the type-II InGaN–GaNAs QW structure can be attributed to the improved hole wave function confinement from the use of GaNAs layer, leading toward the improvement in its electron-hole wave function overlap (Γ_{e_hh}). For the case of $n=2\times10^{19}$ cm^{-3}, the Γ_{e_hh} of the type-II QW structure is 60.93%, which is 1.74 times higher than that ($\Gamma_{e\_hh}=35.02\%$) of conventional InGaN QW.

The spontaneous emission rate per unit volume R_{sp}(s^{-1} cm^{-3}) can be obtained by integrating the spontaneous emission spectra (Fig. 4) over the entire frequency region. The radiative current density (J_{rad}) can be obtained from the spontaneous emission recombination rate as follows:

$$J_{rad}=qdR_{sp}. \tag{2}$$

The comparison of the radiative current density (J_{rad}) for both type-II InGaN–GaNAs QW and conventional type-I InGaN QW is shown in Fig. 5. The use of type-II QW active region shows a significant enhancement in the radiative current density, which is consistent with the larger radiative recombination rate in the type-II QW structure. At carrier density $n=4\times10^{19}$ cm^{-3}, the radiative current density for type-II is computed as $J_{rad}=253.7$ A/cm^2, which is 133.6% larger than that ($J_{rad}=108.6$ A/cm^2) of conventional type-I InGaN QW.

VI. OPTICAL GAIN AND DIFFERENTIAL GAIN OF TYPE-II INGAN–GANAS QW

The optical gain spectra were calculated self-consistently for both the type-I InGaN QW structure and the type-II InGaN–GaNAs QW structure with carrier density (n) rang-

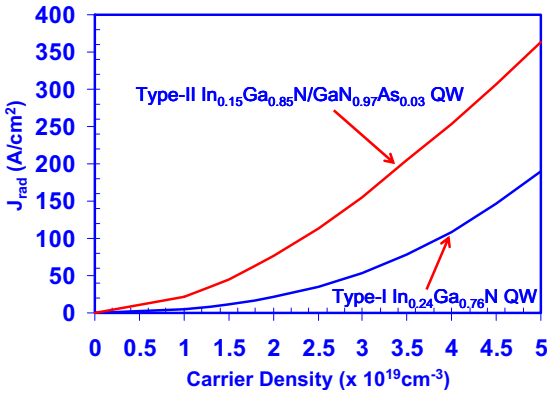

FIG. 5. (Color online) Radiative current density (J_{rad}) as a function of carrier density for type-I $In_{0.24}Ga_{0.76}N$ QW and type-II $In_{0.15}Ga_{0.85}N-GaN_{0.97}As_{0.03}$ QW.

ing from 2×10^{19} up to 5×10^{19} cm^{-3} at $T=300$ K, as shown in Fig. 6. From our studies, the type-II InGaN–GaNAs QW structure exhibits improvement in optical gain in comparison to that of the type-I InGaN QW structure. Note that both QWs were designed as active regions for diode lasers with emission wavelength at $\lambda\sim460$ nm, for near-threshold condition $[n_{th}\sim(2.4-3.8)\times10^{19}$ $cm^{-3}]$.

Figure 7 illustrates the comparison of the peak gain as a function of the carrier density for the type-I $In_{0.24}Ga_{0.76}N$ QW and type-II $In_{0.15}Ga_{0.85}N-GaN_{0.97}As_{0.03}$ QW at $T=300$ K, for carrier densities up to $n=5\times10^{19}$ cm^{-3}. The transparency carrier density for the type-I QW of $n_{tr}\sim1.5\times10^{19}$ cm^{-3} is slightly higher than that of the type-II QW of $n_{tr}\sim1.3\times10^{19}$ cm^{-3}. The peak gain for the type-II InGaN–GaNAs QW is increased significantly as a result of its improved transition matrix element. At carrier density $n=4\times10^{19}$ cm^{-3}, the peak gain (g_p) for the type-II InGaN–GaNAs QW is found as 3062.4 cm^{-1}, which is a 1.85 times improvement as compared to that ($g_p=1657.5$ cm^{-1}) of the type-I InGaN QW.

The comparison of the differential gain (dg/dn) of both type-I and type-II QW is shown in Fig. 8, for carrier densities up to $n=5\times10^{19}$ cm^{-3}. From our studies, the differential gain (dg/dn) for the type-II InGaN–GaNAs QW is found

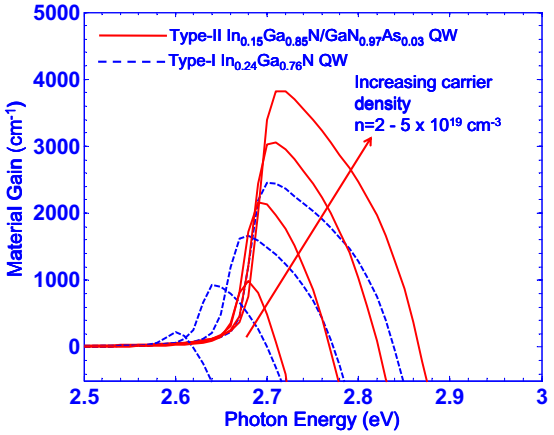

FIG. 6. (Color online) Optical gain spectra for type-I $In_{0.24}Ga_{0.76}N$ QW and type-II $In_{0.15}Ga_{0.85}N-GaN_{0.97}As_{0.03}$ QW as increasing carrier density $n=(2-5)\times10^{19}$ cm^{-3} with self-consistent model calculation.

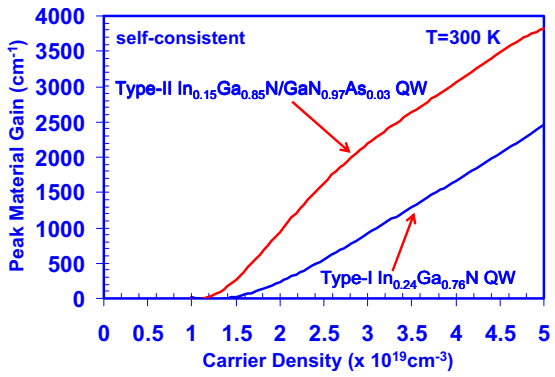

FIG. 7. (Color online) Peak material gain (g_p) as a function of carrier density for type-I $In_{0.24}Ga_{0.76}N$ QW and type-II $In_{0.15}Ga_{0.85}N-GaN_{0.97}As_{0.03}$ QW at room temperature.

as larger than that of the type-I InGaN QW for all carrier density regimes. Note that the trend of the differential gain for type-II InGaN–GaNAs QW is different from that of the type-I InGaN QW. Near the transparency carrier density, the differential gain for the type-II QW increases to a maximum value ($dg/dn=14.5\times10^{-17}$ cm^2) at carrier density $n=1.86\times10^{19}$ cm^{-3}. Beyond the peak dg/dn condition, the differential gain of the type-II QW decreases gradually. For the case of type-I InGaN QW, the differential gain increases slowly near the transparency, and then reaches a stable value of $(7.1-7.4)\times10^{-17}$ cm^2 for a carrier density range of $n=(2.5-3.5)\times10^{19}$ cm^{-3}. The observed improvement in the optical gain and differential gain in the type-II InGaN–GaNAs QW is important in particular to achieve low threshold carrier density in laser diode operation. The use of type-II InGaN–GaNAs QW active region will lead to a significant reduction in the threshold carrier density to achieve a low threshold carrier density (n_{th}), which in turn leads to a suppression in the nonradiative recombination current density.

VII. THRESHOLD ANALYSIS OF TYPE-II INGAN–GANAS QW LASERS

To evaluate the feasibility of the type-II $In_{0.15}Ga_{0.85}N-GaN_{0.97}As_{0.03}$ QW as active region emitting at 460 nm for diode lasers and compare the performance with

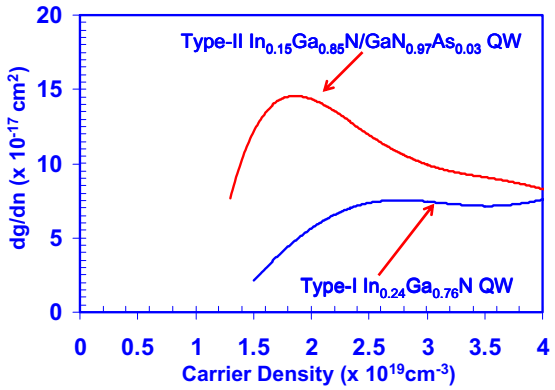

FIG. 8. (Color online) Differential gain (dg/dn) as a function of carrier density for type-I $In_{0.24}Ga_{0.76}N$ QW and type-II $In_{0.15}Ga_{0.85}N-GaN_{0.97}As_{0.03}$ QW at room temperature.

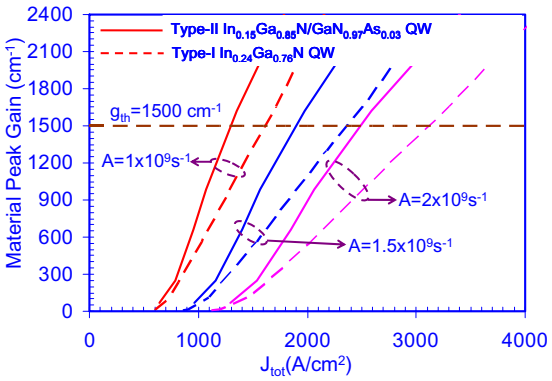

FIG. 9. (Color online) Peak material gain (g_p) as a function of current density (J_{total}) for type-I $In_{0.22}Ga_{0.78}N$ QW and type-II $In_{0.15}Ga_{0.85}N-GaN_{0.97}As_{0.03}$ QW at room temperature.

the conventional type-I InGaN QW emitting at the same wavelength, we employed a single QW active region in a nitride-based laser structure similar to the structure fabricated in Ref. 32. The optical confinement factor (Γ_{opt}) and internal loss (α_i) for this structure are 0.01 and 10.15 cm^{-1}, respectively. By using the cavity length of 650 μm and end facet reflectivity of 95%/56% (corresponding to mirror loss $\alpha_m=4.85$ cm^{-1}),[32] the calculated threshold gain (g_{th}) for laser application is ~ 1500 cm^{-1}. Attributing to the higher differential gain (dg/dn) and lower transparency carrier density (n_{tr}) in type-II QW, the threshold carrier density of type-II InGaN–GaNAs QW is considerably lower than that of conventional type-I InGaN QW. The threshold carrier density for the type-II QW is 2.4×10^{19} cm^{-3}, which shows a 36.8% reduction as compared to that (3.8×10^{19} cm^{-3}) of the type-I QW. Note that for the nonradiative recombination current density, we only consider the monomolecular recombination current density ($J_{mono}=A\,n$), where A is the monomolecular recombination constant. For wide band gap material system, the Auger recombination process is negligible due to the small value of the Auger recombination rate [$C_{Auger}=(0.9-1)\times10^{-32}$ cm^6/s].[33] The reduced threshold carrier density is important to suppress the nonradiative current density (J_{nonrad}), and then reduce the total threshold current density ($J_{tot}=J_{rad}+J_{nonrad}$).

Figure 9 shows the optical gain versus the threshold current density for both type-I and type-II InGaN QWs with three different monomolecular recombination constants,[34] as follows: $A=1\times10^9$ s^{-1}, $A=1.5\times10^9$ s^{-1}, and $A=2\times10^9$ s^{-1}. The comparison for the threshold current densities for three different monomolecular coefficients is shown in Table II. By using the type-II QW structure, the threshold current density is reduced by $\sim$20%. The reduced J_{th} for the type-II InGaN QW is a consequence of the higher electron-hole wave function overlap leading to reduced threshold carrier density, which in turn leads to the suppression in nonradiative recombination current density. The type-II QW has the potential to be applied to laser structure with low transparency and threshold carrier densities, high optical gain and differential gain, and low threshold current density.

In our threshold analysis here, we have neglected the contribution of Auger recombination current density ($J_{mono}=C_{Auger}\,n^3$) due to the small theoretical Auger coefficient

TABLE II. The total threshold current density (J_{th_total}) for type-I $In_{0.24}Ga_{0.76}N$ QW and type-II $In_{0.15}Ga_{0.85}N-GaN_{0.97}As_{0.03}$ QW with various monomolecular recombination rates (A).

Monomolecular recombination coefficient (A)	Total threshold current density (J_{th_total}) for type-II InGaN–GaNAs QW (A/cm^2)	Total threshold current density (J_{th_total}) for type-I InGaN–GaN QW (A/cm^2)
$A=1\times10^9$ s^{-1}	1305	1605
$A=1.5\times10^9$ s^{-1}	1900	2350
$A=2\times10^9$ s^{-1}	2500	3100

[$C_{Auger}=(0.9-1)\times10^{-32}$ cm^6/s] (Ref. 33) in the large band gap InGaN material system. However, it is important to note that recent reports by Shen *et al.*[35] indicated that Auger recombination coefficient (C_{Auger}) in InGaN / GaN QW system as $(1.4-2)\times10^{-30}$ cm^6/s,[35] which is approximately two orders of magnitude larger than the theoretical value. Further studies are still required to clarify the inconsistencies in the reported Auger coefficients in InGaN QW system.[33,35]

If Auger recombination is taken into consideration, then the nonradiative current density is composed of two parts ($J_{non}=J_{mono}+J_{Auger}$), which are monomolecular recombination current density ($J_{mono}=A\,n$), and Auger recombination current density ($J_{Auger}=C_{Auger}\,n^3$). Therefore, a significant reduction in the threshold carrier density (n_{th}) by using the type-II InGaN–GaNAs QW will be crucial for suppressing the J_{Auger}. By utilizing the type-II InGaN–GaNAs QW, the Auger recombination current will be reduced by $\sim$74.8% as compared to the conventional InGaN QW.

VIII. SUMMARY

In summary, type-II $In_{0.15}Ga_{0.85}N-GaN_{0.97}As_{0.03}$ QW was analyzed self-consistently as improved gain media for nitride-based diode lasers emitting at $\lambda\sim460$ nm. The energy dispersion relations were calculated using a self-consistent six-band $\boldsymbol{k}\cdot\boldsymbol{p}$ formalism, taking into account the valence band mixing, strain effect, polarization fields, and carrier screening effects. Attributing to the improved matrix element of the type-II InGaN–GaNAs QW, its spontaneous emission and optical gain indicate significant improvements in comparison to that of conventional InGaN QW. The differential gain of the type-II InGaN–GaNAs QW is also improved, while its transparency carrier density is reduced by 15.4%. The optical gain of the type-II InGaN–GaNAs QW is improved by approximately 2 times over that of the conventional InGaN QW, resulting in a reduction in threshold carrier density and threshold current density by $\sim$36.8% and 20%, respectively. Thus, the use of type-II InGaN–GaNAs QW as active region can be advantageous for achieving low threshold diode lasers and high-efficiency nitride-based LEDs.

ACKNOWLEDGMENTS

The authors acknowledge supports from National Science Foundation (Contract No. 0701421), Department of Energy, and P. C. Rossin Professorship Funds.

[1]S. Nakamura, M. Senoh, N. Iwasa, S. Nagahama, T. Yamada, and T. Mukai, Jpn. J. Appl. Phys., Part 2 **34**, L1332 (1995).
[2]S. Nakamura, M. Senoh, S. Nagahama, N. Iwasa, T. Yamada, T. Matshushita, H. Kiyoku, and Y. Sugimoto, Jpn. J. Appl. Phys., Part 2 **35**, L74 (1996).
[3]E. F. Schubert, *Light Emitting Diodes*, 2nd ed. (Cambridge University Press, Cambridge, England, 2006).
[4]S. Nagahama, Y. Sugimoto, T. Kozaki, and T. Mukai, Proceedings of SPIE Photonics West, San Jose, CA, January 2005.
[5]R. M. Farrell, D. F. Feezell, M. C. Schmidt, D. A. Haeger, K. M. Kelchner, K. Iso, H. Yamada, M. Saito, K. Fujito, D. A. Cohen, J. S. Speck, S. P. DenBaars, and S. Nakamura, Jpn. J. Appl. Phys., Part 2 **46**, L761 (2007).
[6]J. Park and Y. Kawakami, Appl. Phys. Lett. **88**, 202107 (2006).
[7]S. H. Park, J. Park, and E. Yoon, Appl. Phys. Lett. **90**, 023508 (2007).
[8]R. A. Arif, Y.-K. Ee, and N. Tansu, Appl. Phys. Lett. **91**, 091110 (2007).
[9]R. A. Arif, H. Zhao, Y.-K. Ee, and N. Tansu, IEEE J. Quantum Electron. **44**, 573 (2008).
[10]R. A. Arif, Y.-K. Ee, and N. Tansu, Phys. Status Solidi C **205**, 96 (2008).
[11]H. Zhao, R. A. Arif, Y. K. Ee, and N. Tansu, Opt. Quantum Electron. **40** (May 2008).
[12]H. Zhao, R. A. Arif, Y. K. Ee, and N. Tansu, in Proceedings of the SPIE Photonics West 2008: Physics and Simulation of Optoelectronics Devices XVI, San Jose, CA, 2008, Vol. 6889, p. 688903.
[13]H. Zhao, R. A. Arif, Y. K. Ee, and N. Tansu, IEEE J. Quantum Electron. **44** (October 2008).
[14]R. A. Arif, H. Zhao, and N. Tansu, Appl. Phys. Lett. **92**, 011104 (2008).
[15]J. R. Meyer, C. A. Hoffman, F. J. Bartoli, and L. R. Ram-Mohan, Appl. Phys. Lett. **67**, 757 (1995).
[16]I. Vurgaftman, C. L. Felix, W. W. Bewley, D. W. Stokes, R. E. Bartolo, and J. R. Meyer, Philos. Trans. R. Soc. London, Ser. A **359**, 489 (2001).
[17]N. Tansu and L. J. Mawst, IEEE J. Quantum Electron. **39**, 1205 (2003).
[18]I. Vurgaftman, J. R. Meyer, N. Tansu, and L. J. Mawst, Appl. Phys. Lett. **83**, 2742 (2003).
[19]J. Y. Yeh, L. J. Mawst, A. A. Khandekar, T. F. Kuech, J. R. Meyer, I. Vurgaftman, and N. Tansu, Appl. Phys. Lett. **88**, 051115 (2006).
[20]I. Vurgaftman, J. R. Meyer, N. Tansu, and L. J. Mawst, J. Appl. Phys. **96**, 4653 (2004).
[21]S. L. Chuang and C. S. Chang, Semicond. Sci. Technol. **12**, 252 (1997).
[22]A. Kimura, C. A. Paulson, H. F. Tang, and T. F. Kuech, Appl. Phys. Lett. **84**, 1489 (2004).
[23]J. Wu, W. Walukiewicz, K. M. Yu, J. D. Denlinger, W. Shan, J. W. Ager III, A. Kimura, H. F. Tang, and T. F. Kuech, Phys. Rev. B **70**, 115214 (2004).
[24]S. L. Chuang, IEEE J. Quantum Electron. **32**, 1791 (1996).
[25]F. Bernardini and V. Fiorentini, Phys. Status Solidi B **216**, 391 (1999).
[26]J. Piprek, *Semiconductor Optoelectronic Devices: Introduction to Physics and Simulation* (Academic, London, 2003), p. 34.
[27]J. Wu, W. Walukiewicz, W. Shan, K. M. Yu, J. W. Ager III, S. X. Li, E. E. Haller, H. Lu, and W. J. Schaff, J. Appl. Phys. **94**, 4457 (2003).
[28]J. Piprek and S. Nakamura, IEE Proc.-J: Optoelectron. **149**, 145 (2002).
[29]I. Vurgaftman and J. R. Meyer, in *Nitride Semiconductor Devices*, edited by J. Piprek (Wiley, New York, 2007), Chap. 2.
[30]I. Vurgaftman and J. R. Meyer, J. Appl. Phys. **94**, 3675 (2003).
[31]Y. C. Yeo, T. C. Chong, M. F. Li, and W. J. Fan, J. Appl. Phys. **84**, 1813 (1998).
[32]H. Y. Ryu, K. H. Ha, S. N. Lee, T. Jang, J. K. Son, H. S. Paek, Y. J. Sung, H. K. Kim, K. S. Kim, O. H. Nam, Y. J. Park, and J. I. Shim, IEEE Photon. Technol. Lett. **19**, 1717 (2007).
[33]J. Hader, J. V. Moloney, A. Thranhardt, and S. W. Koch, in *Nitride Semiconductor Devices*, edited by J. Piprek (Wiley, Weinheim, Germany, 2007), Chap. 7, p. 164.
[34]W. W. Chow and M. Kneissl, J. Appl. Phys. **98**, 114502 (2005).
[35]Y. C. Shen, G. O. Mueller, S. Watanabe, N. F. Gardner, A. Munkholm, and M. R. Krames, Appl. Phys. Lett. **91**, 141101 (2007).